International Journal of Bioprinting

RESEARCH ARTICLE

Tissue-engineered edible bird's nests (TeeBN)

Yu Liu[1†], Yangyang Liu[1†], Jiayue Liu[1], Yuwei Li[1], Jian-Bo Wan[1], Yiming Niu[1], Lei Dong[2], Li Du[3], Chunming Wang[1,4*]

[1]State Key Laboratory of Quality Research in Chinese Medicine, Institute of Chinese Medicine & Department of Pharmaceutical Sciences, Faculty of Health Science, University of Macau, Taipa, Macau SAR

[2]State Key Laboratory of Pharmaceutical Biotechnology, School of Life Sciences, Nanjing University, Nanjing, Jiangsu, 210093, China

[3]Faculty of Law, University of Macau, Taipa, Macau SAR

[4]Zhuhai UM Science & Technology Research Institute (ZUMRI), University of Macau, Hengqin, Guangdong, China

(This article belongs to the *Special Issue: Advances in 3D bioprinting for regenerative medicine and drug screening*)

Abstract

Edible bird's nests (EBN)—the nests of swiftlet birds harvested from the wild—are high-end healthcare food in East Asia, while their excessive harvesting poses increasing ecological, environmental, and food safety concerns. Here, we report for the first time a tissue-engineering (TE) approach for fabricating EBNs substitutes by integrating the technologies of three-dimensional (3D) printing and live cell culture. The engineered products, tissue-engineered edible bird's nests (TeeBN), comprise two layers. The first is a feeding layer that encapsulates epithelial cells in 3D-printed biocompatible gelation scaffolds. These cells secrete bioactive ingredients, e.g., sialic acid and epidermal growth factors (EGF), recapitulating the natural production of these substances by birds. The second is a receiving layer, consisting of food-grade natural polymers, e.g., polysaccharides, which mimics the building blocks of natural EBNs while biologically stabilizing the factors released from the feeding layer. *In vitro* characterizations demonstrate that the feeding layer facilitates 3D cell growth and functions, and the receiving layer (as the end product) contains the necessary nutrients expected from natural EBNs—while without harmful substances commonly detected in natural EBNs. Further, *in vivo* metabolomics studies in mice indicate that TeeBN showed a similar profile of serum metabolites as natural EBN, reflecting comparable nutritional effects. In summary, we innovatively developed a tissue engineering-based substitute for EBNs with comparable metabolic functions and minimized safety risks, opening a new avenue for producing delicacy food from laboratorial cell culture with 3D printing technology.

Keywords: Tissue engineering; 3D printing; Cellular agriculture; Food technology; Edible bird's nests

1. Introduction

Edible bird's nests (EBN), the nests of swiftlet birds made of solidified saliva, have been consumed as a delicacy food in East Asia for centuries[1]. Their "health-promoting effects"

†These authors contributed equally to this work.

***Corresponding author:**
Professor Chunming Wang
(cmwang@umac.mo)

Citation: Liu Y, Liu Y, Liu J, *et al*., 2023, Tissue-engineered edible bird's nests (TeeBN). *Int J Bioprint*. https://doi.org/10.18063/ijb.691

Received: October 11, 2022
Accepted: November 16, 2022
Published Online: February 21, 2023

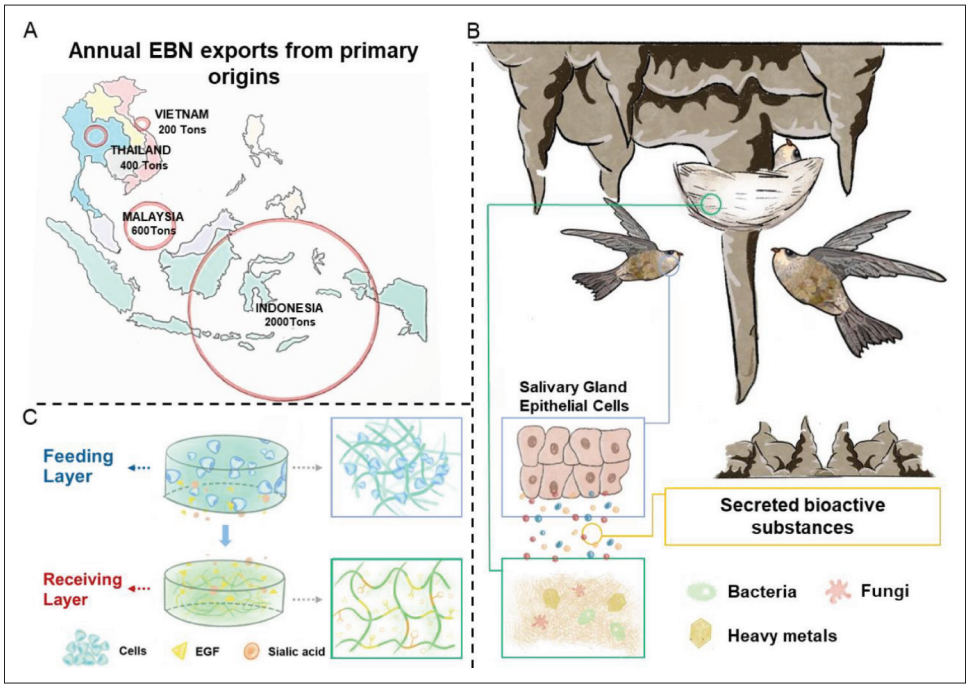

Figure 1. Producing replacements for EBN with the tissue-engineering methodology has both environmental and economic impacts. (A) The huge demand for harvesting wild EBN in Southeast Asia damages the swiftlets' home and the local ecological system. (B) Illustration of natural EBN's formation, containing both nutritional components secreted from the birds' epithelial cells and hazard substances like microbes and heavy metals. (C) Scheme of reproducing EBN formation with biomaterials, with a feeding layer (upper) of 3D-printed matrix culturing epithelial cells to produce functional ingredients to be enriched in a receiving layer (lower) composed of food-grade materials. The receiving layer, representing the TeeBN, contains the essential nutritional factors of natural EBN while avoiding heavy metal and microbial contaminations normally occurring in the latter.

supported by traditional Chinese medicine guarantee a USD 6.5 billion market in China alone and a rising international market prices up to USD 6,600 per kilogram[2-5]. However, the rapidly increasing demand for EBN has triggered serious ecological and social issues. The annual export volume from major producing countries in Southeast Asia exceeds 3,000 tons (Figure 1A). Excessive harvesting and unsustainable farming irreversibly damage the environment, rendering 4 million birds homeless and endangering certain swallow species[6,7]. Also, natural EBNs on the market are often detected with toxic heavy metal salts and microbial contamination[8]. Some products rich in nitrous acids and hence appearing red are portrayed and overpriced as the rarest "blood bird's nests," with no scientific evidence except for potential adverse effects from sodium nitrite ($NaNO_2$) [8,9]. Although government authorities and non-government organizations have tried establishing artificial caves and large-scale breeding, these attempts are regionally limited and loosely regulated. Producing EBN in an environmentally friendly and sustainable manner has emerged as a pressing challenge for both environmental protection and food security[6].

Tissue engineering (TE)—a medical technology to regenerate the human body—may provide an unexpected answer to this challenge. TE promises to repair diseased tissue by *in vitro* culturing mammalian cells in three-dimensional (3D) biomaterials scaffolds to develop functional tissue, with notable clinical breakthroughs in the cartilage, bone, and skin, among other tissue types[10]. In fact, it is often overlooked that the natural production of EBN by swiftlets is also a physiological function of live tissue. The bird's saliva gland cells secrete saliva, which solidifies to form the bowl nests adhering to the cave wall for the birds' habitation until being harvested for human consumption (Figure 1B)[1]. The nests contain abundant proteins and carbohydrates (>50% and >30% dry weight, respectively) produced by salivary epithelial cells, which are believed to be the main nutritional ingredients that underpin the healthcare effects of EBN[11]. Utilizing the TE methodology to recapitulate the process of EBN production *in vitro* might open a new avenue for engineering environmentally friendly EBN.

The key to realizing this goal is to ensure the engineered EBN contains the essential nutritional ingredients of natural EBN in two main categories—(i) the structural macromolecules (e.g., glycans), which can be mimicked with existing food-grade materials, and (ii) the small-molecule metabolites and growth factors secreted by the salivary gland, e.g., epithelial growth factor (EGF), sialic acid, and *N*-acetylneuraminic acid, which are hard to mimic and should ideally be released by living epithelial

cells[2,12]. A possible design is to culture salivary gland cells in one layer-TE-based simulation of the bird's salivary gland and construct another biomaterials layer to collect and stabilize the nutritional components from the first layer. The first layer should facilitate the optimal survival and secreting function of salivary gland cells and efficient diffusion of molecules; the second layer should serve as the engineered EBN product for consumption.

Based on the above assumption, we proposed to devise a two-layer model for this "tissue-engineered" EBN (TeeBN). For the first "feeding layer," we synthesized gelatin methacrylate (GelMA) and employed 3D printing to encapsulate submandibular gland epithelial cells (SGEC) in GelMA hydrogels. The 3D-printed gel created a biomimetic niche for the cells to survive—a typical TE setting—and continuously release nutritional factors. Then, we reconstituted food-grade glycan materials according to the carbohydrate proportions of natural EBN into the second "receiving layer," which both provided the ingredients and, more importantly, stabilized EGF released from the feeding layer through carbohydrate-growth factor interaction (Figure 1C). After constructing this TeeBN model, we analyzed its biochemical parameters *in vitro* and tested its metabolism *in vivo*, with emphases on how it could retain the essential nutritional factors of natural EBN, while avoiding heavy metal and microbial contaminations normally present in the latter.

2. Materials and methods

2.1. Synthesis of methacrylate gelatin (GelMA)

Gelatin (10 g; Sigma Aldrich, Burlington, USA) was fully dissolved in phosphate-buffered saline (PBS, 10 mL; Gibco, Waltham, USA) at 50°C for 3 h. By referring to a previously reported method[13], methacrylic anhydride (MA, 8 mL; Sigma Aldrich, Burlington, USA) was slowly added to the gelatin solution in a round-bottom flask. Then, the methacrylate gelatin samples were dialyzed against deionized water (molecular weight cut-off: 12–14 kDa) at 40°C for 1 week, before being frozen and lyophilized. The synthesized GelMA was verified by ^{1}H-NMR[14].

2.2. Cell culture

Murine submandibular gland epithelial cells (MSGEC) were purchased from YuchiCell (Shanghai, China) and cultured with the DMEM (Gibco, Waltham, USA) with 10% (v/v) fetal bovine serum (Gibco, Waltham, USA), 1% (v/v) GlutaMax (Gibco, Waltham, USA), and 1% (v/v) antibiotics (Gibco, Waltham, USA). Incubator parameters were set at 37°C and 5% carbon dioxide.

2.3. Flow and temperature sweep of GelMA

The modulus of GelMA samples was analyzed by Discovery HR-2 rheometer (TA Instruments, New Castle, USA) following a previously described method[15]. For flow sweep, the rheology study was carried out at room temperature. A parallel plate with a diameter of 20 mm and a truncation gap distance of 1,000 μm was applied to all GelMA samples. To measure the viscosity, these GelMA samples were loaded with steady rate sweeps within a shear rate range of 0.01–1,000 s^{-1}. The sweep points were set with 10 per decade, and the angular frequency ranged from 0.1–100.0 rad s^{-1}. For temperature sweep, to measure the storage modulus and loss modulus, GelMA samples were loaded with steady rate sweeps within a shear rate range of 0.01–1,000 s^{-1}. The sweep points were set at 10 per decade. To measure the storage modulus (G′) and loss modulus (G″) in the temperature ranging from 22°C to 40°C, temperature sweep tests were conducted in the linear viscoelastic region at a strain of 1%.

2.4. 3D printing of the feeding layer

The BioScaffolder BS3.2 (GeSiM, Radeberg, Germany) was used to print the feeding layer. Before cell loading, a total of 91 GelMA samples were tested to draw the printability window, with the temperature ranging from 22°C to 28°C and the pressure from 10 to 130 kPa. GelMA ink, with 0.25% (w/v) photoinitiator lithium phenyl-2, 4, 6-trimethyl-benzoyl phosphinate (LAP), was loaded into preheated cartridges (26°C) and printed at 4 mm/s through a 27 G, 410 μm conical needle to a cooled receiving platform (4°C). The final hydrogel scaffold was crosslinked under 405 nm blue light for 10 s. 3D models for grids and discs were processed with GeSiM Robotics version 1.16.0.3892[15].

For cell-loaded printing, 1 g GelMA was dissolved in 10 mL PBS containing 0.25% (w/v) LAP and filtered by 0.22 μm filtration membrane to finally obtain a 10% (w/v) concentration GelMA as the biomaterial ink. Epithelial Cells (5×10^6 cells/mL) were mixed with 1 mL biomaterial ink. After printing, the medium was soaked for 5 min and then replaced with the complete medium culture in the incubator.

2.5. Cytotoxicity of GelMA scaffolds

Epithelial cells (5×10^3 cells/mL) were cultured with GelMA scaffolds soaking medium in 96-well plates, followed by testing in CCK-8 cell viability assay (ApexBio, Houston, USA) after 1, 3, and 5 days. The working solution consisted of staining solution and medium at 1:10 (v/v). After a 4-h culture, the absorbance (450 nm) was measured using a microplate reader (Molecular Devices, San Jose, USA)[16].

2.6. Assays to evaluate cell growth in the feeding layer

Live/Dead assay (Sigma Aldrich, Burlington, USA) was performed to observe the impact of different feeding layers on epithelial cells[16]. The dye was applied 1/1,000 (v/v) of

the medium. After a 1-h culture, the cells were observed under an inverted fluorescence microscope (Leica Dmi 8, Morrisville, USA).

The cell-loading rate in different models was compared. In the 2D surface group, 500 μL of GelMA was added to 2 cm^2 (24 well plate) and photo-crosslinked, forming a 2D surface available for cell culture. In 3D encapsulation group, 500 μL GelMA loaded with cells was crosslinked, whereas in 3D printing group, 500 μL GelMA was loaded with cells and grid printed before crosslinking. The cell density was controlled across different experimental groups to obtain a 70% field of view under the microscope to mimic the cell density in the logarithmic growth phase. Finally, the cells were collected and the total number of cells was calculated to assess the cell loading rate.

EdU assay was employed to assess epithelial cell proliferation (BeyoClick™ Cell Proliferation Kit with Alexa Fluor 594, Beyotime, Shanghai, China)[17]. Briefly, the different feeding layers were cultured with DMEM containing 10 μM EdU for 12 h. Following cell fixation using 4% (w/v) paraformaldehyde, cells were incubated with staining working buffer for 1 h before being co-stained with DAPI for 10 min. ImageJ (NIH, Bethesda, USA) was used to count the total number of cells and the number of positive cells separately.

In gene expression studies, RNA from cells cultured in different feeding layer models were obtained via Trizol (Beyotime, Shanghai, China) extraction. A total of 2 μg of cDNA was collected by All-in-One MasterMix (abm, Vancouver, Canada). Then, real-time polymerase chain reaction (PCR) was performed on CFX-96 Touch™ (BioRad, Hercules, USA) using the GoTaq®qPCR Master Mix kit (Promega, Madison, USA)[18]. Glyceraldehyde 3-phosphate dehydrogenase (GAPDH) was used as the housekeeping gene and the relative expression of genes was calculated by $2^{-\Delta\Delta Ct}$. The primers are listed in **Table S1.**

Cell morphology was observed by the Alexa Fluor 488 Phalloidin Cytoskeleton staining kit (ThermoFisher, Waltham, USA). Briefly, after being cultured for 24 h, the feeding layer was washed once with PBS. Fixation and permeation were performed using 4% paraformaldehyde for 30 min and Triton X-100 (Beyotime, Shanghai, China) for 10 min. Phalloidin (1:500) was added for 1 h before the cells were stained with DAPI for 10 min at room temperature. Finally, the feeding layer was washed three times with PBS and observed under an inverted fluorescence microscope (Leica Dmi 8, Morrisville, USA).

2.7. Dot blotting of EGF and hyaluronic acid (HA)

Three kinds of HA with different molecular weights (L-HA: 10–20 kDa, M-HA: 40–80 kDa, and H-HA: 100–150 kDa; Aladdin, Shanghai, China) were prepared in three concentrations as 1.25 mg/mL, 2.5 mg/mL, and 5 mg/mL, respectively. Recombinant proteins of meiyo epidermal growth factor (EGF; Boster, Shanghai, China) were prepared in 25 μg/mL, 50 μg/mL, and 100 μg/mL. The HA samples were added to the polyvinylidene difluoride (PVDF) membrane by dropping 50 μL in the order of concentration[16]. After drying, the membrane was immersed in 5% bovine serum albumin (BSA) for 1 h. Then, the PVDF membrane was incubated with EGF at 37°C for 3 h, washed three times with PBS, blocked in 5% BSA for 1 h, and subsequently incubated with the primary antibody (anti-EGF; Boster, Shanghai, China) in 1% BSA overnight at 4°C. Secondary antibodies in 1% BSA were incubated for another 1 h at room temperature. After rinsing with PBS, the HA-EGF binding was detected with SuperSignal West Pico Chemiluminescent Substrate (Thermos Scientific, Waltham, USA).

2.8. Preparation of receiving layer

H-HA and gelatin were the main components of the receiving layer of TeeBN. To simulate the functional components of natural EBN[11,19], we constituted carbohydrate ingredients to adjust the proportion of the final composing monosaccharides, as illustrated in composition table of Figure 3A. For the receiving layer, all the materials used are of food-grade quality.

2.9. Scanning electron microscope (SEM)

The morphology of the receiving layer was characterized by a high-resolution SEM JSM-6700F (JEOL, Tokyo, Japan). After freeze-drying, the sample was fixed on the specimen platform and coated with gold for SEM observation[18].

2.10. Heavy metal assay

Heavy metals (As, Pb, Cu) in EBN and TeeBN (receiving layer) were measured by inductively coupled plasma mass spectrometry (ICP-MS) (Thermo Scientific, Waltham USA) by referring to the previously reported method[20]. The samples (0.2 g) were weighed and placed in a polytetrafluoroethylene (PTFE) digestion tank, and 8 mL of 65% nitric acid was added as a digestive solution. At first, the samples were placed in the microwave digestion apparatus for a 20-min pre-digestion. Next, the samples were subjected to acidic gas evaporation on the heating plate at 120°C for 3 min and the remaining sample solution was diluted to 25 mL with deionized water. A standard curve was drawn for each ICP-MS assay. Finally, the nitrite content in the sample was calculated and obtained.

2.11 Nitrite quantification

Nitrite quantification was determined by iodometry titration[21]. The 100 mg sample dissolved in 50 mL of PBS and the pH value was adjusted to 4, an excess of 0.01 mg/mL

potassium iodide was added and reacted for 4 min, sodium thiosulfate was dropped until the color turned from yellow to light yellow, then 4 mL of 0.5 % starch solution was added dropwise, and sodium hyposulfite was continuously added until the blue color turned to colorless. Finally, the nitrite content in the sample was calculated and obtained.

2.12. Determination of sialic acid, EGF, and total proteins

EBN and TeeBN with a dry weight of 1 g was weighed and dissolved in 1 mL of deionized water. Sialic acid quantitation was performed by Sialic Acid Assay Kit (Sigma Aldrich, Burlington, USA). Briefly, following the improved Warren's method, sialic acid was calculated by colorimetric (549 nm)/ fluorometric (λex = 555 nm/ λem = 585 nm)[22].

Mouse EGF concentrations were determined by the enzyme-linked immunosorbent assay kit (ELISA; Cusabio, Wuhan, China). Briefly, culture supernatants of the feeding layer or EBN and TeeBN were collected and transferred to anti-EGF-coated wells. Working buffer was added according to the protocol and absorbance (450 nm) was measured using the microplate reader (Molecular Devices, San Jose, USA).

Total protein was quantitated by the BCA protein assay kit (Beyotime, Shanghai, China)[16]. Each sample was treated with BCA working buffer for 2 h at room temperature and absorbance (562 nm) was measured using the microplate reader (Molecular Devices, San Jose, USA).

2.13. Metabolomics

EBN and TeeBN samples for metabolomics analysis were sourced from Indonesia[23,24]. Methanol-water solution (400 μL) was added to a 100 μL of EBN or TeeBN sample. The mixture then went through a vortex for 30 s and was sonicated at 40 kHz for 30 min at 5°C. Next, the samples were placed at -20°C for 30 min to precipitate proteins. After being centrifuged at 13,000 × *g* and 4°C for 15 min, the supernatant was transferred for ultra-high performance liquid chromatography-MS/MS (UHPLC-MS/MS) analysis. A Thermo UHPLC system equipped with an ACQUITY BEH C18 column (length: 100 mm; inner diameter: 2.1 mm; grain diameter: 1.7 μm; Waters, Milford, USA) was used to perform chromatographic separation of the metabolites. The mobile phase consisted of 0.1 % (v/v) formic acid in water (phase A) and 0.1% (v/v) formic acid in a mixture of acetonitrile and isopropanol (1:1, v/v) (phase B) at a flow rate of 0.40 mL/min. The elution gradient was used as: 0 to 3.0 min, 5% to 20% phase B; 3.0 to 9.0 min, 20% to 95% phase B; 9.0 to 13.0 min, 95% phase B; 13.0 to 13.1 min, 95% to 5% phase B; 13.1 to 16 min, 5% phase B. The samples were injected at a volume of 2 μL. The column temperature was maintained at 40°C. All samples were stored at 4°C during the analysis period.

The mass spectrometer was performed in negative mode with an electrospray ionization (ESI) ion source. The optimal methods were as follows: heater temperature, 425°C; sheath gas flow rate, 50 arb (arbitrary unit); aux gas flow rate, 13 arb; ion-spray voltage floating (ISVF), -3,500 V in negative mode and 3,500 V in positive mode; normalized collision energy, 20 to 40 to 60 V rolling for MS/MS. Data acquisition was performed from the scan 70 to 1050 m/z.

The UPLC-MS data were analyzed using progenesis QI software (Waters, Milford, USA), with the positive and negative data combined. Metabolites were identified based on the Human Metabolome Database (HMDB) and progenesis QI. Venn plots and heatmaps were used to visualize the significantly changed (Student's *t*-test, $P < 0.05$) metabolites (SCMs) between the EBN and TeeBN groups. Principal component analysis (PCA) and partial least squares-discriminate analysis (PLS-DA) were conducted to identify the SCMs among different groups, with a false discovery rate (FDR) of <0.01 and variable influence on projection (VIP) of >1. Pathway analysis was performed using the Kyoto Encyclopedia of Gene Genotype (KEGG).

2.14. Experimental animals and treatment procedures

This study was reviewed and approved by the Ethics Committee of the University of Macau (UMARE-03-2017 and UMARE-006-2022). All protocols met the requirements of the National Institutes of Health (NIH) Guide for the Care and Use of Laboratory Animals. Eighteen C57BL/6 mice (8 weeks, male) were randomly divided into three groups (n = 6/group): (i) control group, treated by gavage with 0.2 mL of physiological saline; (ii) EBN group, treated by gavage with 0.2 mL of EBN solution; (iii) TeeBN group, treated by gavage with 0.2 mL of TeeBN solution. All mice had regular food and water. All mice received oral gavage for 7 consecutive days. Two hours after the last oral gavage, all mice were anaesthetized and the blood was collected from the eyes. The serum was obtained by centrifugation (3500 × *g*, 10 min) at 4°C and stored at -80°C for use. The preparation and analysis of serum samples for LC-MS were the same as in the EBN and TeeBN metabolomics.

2.15. Statistical analysis

Data are expressed as the mean ± standard deviation (SD). All the experiments were conducted at least three times independently. Statistical significance was determined using one-way and two-way analysis of variance (ANOVA) with Tukey's post hoc multiple comparisons tests in GraphPad Prism 8 (San Diego, USA). In the metabolomics

section, ENB *vs.* TeeBN were analyzed with paired samples *t*-test. Significance was set to $P < 0.05$. ($^{*}P < 0.05$, $^{**}P < 0.01$, $^{***}P < 0.001$, and $^{****}P < 0.0001$)

3. Results and discussion

3.1. Preparation of the feeding-layer material

We aimed to fabricate a 3D matrix of GelMA to encapsulate epithelial cells as the feeding layer (Figure 2A). GelMA is renowned for superior biocompatibility. Despite its commercial availability, we chose to synthesize it in-house in order to fine-tune the mechanical strength, which is vital for printing and epithelial cell survival. We did it by adjusting the substitution ratio of MA to gelatin chains (**Figure S1A**). ^{1}H-NMR confirmed the incorporation of acrylamide double bonds (5.3 and 5.6 ppm) and suggested the degree of methacrylate group at approximately 63% (Figure 2B). In addition, mixing LAP (0.25%, w/v) crosslinker induced rapid crosslinking (<10 s) under blue light (Figure 2C), minimizing the unfavorable environment caused by traditional UV crosslink method (>10 s) influences on cell viability.

Rheological tests showed that the GelMA gel became increasingly viscous as the concentration increased from 1.17 Pa.s of 5% (w/v) to 5.59 Pa.s of 15% (w/v), and the frequency dependence of the energy storage modulus increased with the modification degree (Figure 2D). A 10% concentration could provide adequate mechanical support and avoid being too stiff for the in-gel growth of epithelial cells, which are typical anchorage-dependent cells sensitive to mechanical cues[25]. Measurements of the rheological properties, storage modulus, and loss modulus through temperature scanning identified the window of the gelation state. At room temperature, the energy storage modulus was greater than the loss modulus, and the gel was robust; as the temperature rose to 33°C, the energy storage modulus gradually decreased to the loss modulus, and GelMA briefly presented a gel-state temperature window (**Figure S1B**). The physical state of GelMA is in gel state at this temperature window (22°C–30°C) around room temperature, which is suitable and applicable for extrusion 3D printers and could not significantly affect cell viability[26].

3.2. Cell encapsulation in hydrogel through 3D printing

We fabricated GelMA into hydrogels to encapsulate the epithelial cells through 3D printing. Compared with 2D culture, 3D encapsulation enables a high and controllable cell number to produce sufficient nutritional factors, and printing helps create a tissue-mimicking microenvironment for cell settlement. The GelMA ink for printing should be in appropriate stiffness, avoiding being too hard that could affect the physiological function of the encapsulated cells or being too soft leading to collapse upon fabrication.

Thus, we first explored this printability window by adjusting temperature and pressure and evaluated the pore factor (Pr)[27]. A Pr close to 1 indicates an optimal printing condition. At the same time, its value <1 and >1 suggests the collapse of printing structure and closure of the circle; contrarily, the printing ink is the over concentrated inducing irregular shape of the structure (**Figure S1C**)[15]. After testing 91 combinations, we eventually obtained four categories of conditions: printable, shapeless, congested, and non-printable (Figure 2E); the samples with a Pr around 1 in red rectangles and printing sample shown in Figure 2F.

We then compared the different culturing types to confirm that 3D-printed matrices are optimal for the feeding layer in comparison with 2D surface culture and 3D gel encapsulation (without printing of the porous structure) (Figure 2G). The data showed that the epithelial cells maintained high viability in both 2D surface and 3D printing conditions (>80%) (Live/Dead staining, Figure 2H; quantification, Figure 2I). However, the 3D-printed matrix provided a high cell number per surface area (Figure 2J) and a large proportion of actively proliferating cells (EdU staining; Figure 2K). In comparison, the 2D culture accommodated a limited number of cells while the 3D encapsulation model had both lower viability and fewer proliferating cells. More interestingly, after 7 days of culture, the epithelial cells expressed the highest level of AQP5 (acinar cell-specific marker) and the lowest level of αSMA (myoepithelial marker) in the 3D-printed matrix[28,29], among other cell cycle-related markers (Figure 2L)[30]. This trend was in favor of cell secretory capacity.

Before encapsulation, the cytotoxicity assay (CCK-8) showed that the material, having been rinsed to remove any chemical agents used during the preparation and crosslinking, had no toxicity to epithelial cells (**Figure S1D**) through co-culture with the GelMA soaking solution. After 24-h encapsulation, epithelial cells started to spread in hydrogel network, suggesting that these cells demonstrate their natural morphology in the soft feeding layer (Figure 2M). To verify that the cells could secrete adequately, we chose EGF as the representative nutritional ingredient of EBN and determined its amount by ELISA. The cumulative release data showed increased EGF secretion along the culture time, indicating the functioning of the feeding layer (Figure 2N).

3.3. Preparation of receiving layer

We employed edible hyaluronic acid (HA) as the main structure of the receiving layer. It contains negatively

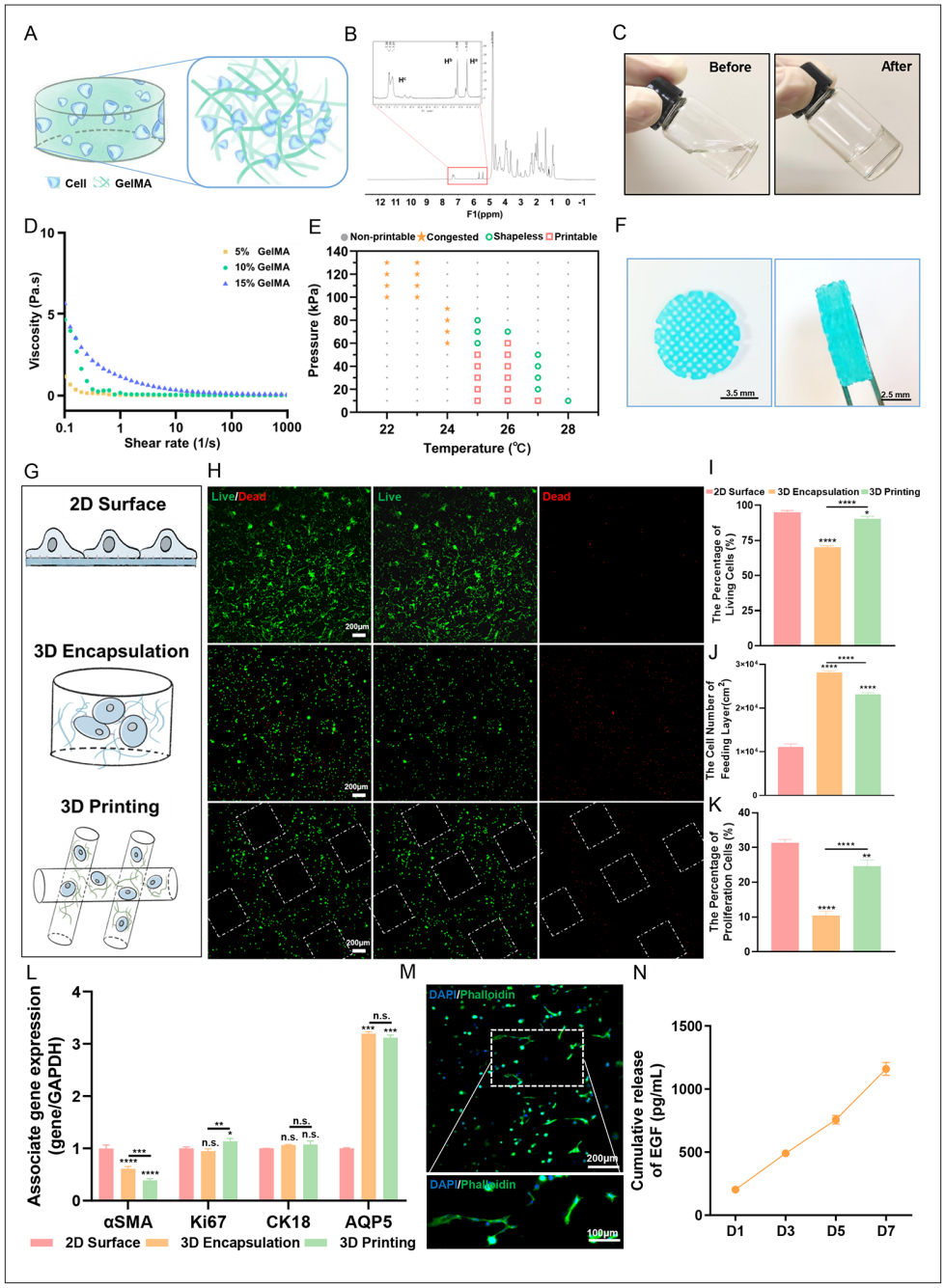

Figure 2. Preparation and evaluation of the feeding layer of TeeBN. (A) Scheme of the feeding layer. (B) ^{1}H-NMR spectrum of GelMA. (C) GelMA solution and GelMA hydrogel formation after photo-crosslinking. (D) The flow sweeps of GelMA with different concentration. (E) Exploring the suitable printing window by Pr values; "non-printable" is defined as "unable to extrude"; "congested" and "over-concentrated" are defined as Pr >1; "collapse" and "forming square structure of ink" are defined as Pr < 1; "printable" is defined as Pr = 1. (F) The feeding layer printing model in printable window. (G) Schematic of different culture models. (H) Live/dead staining of different culture models. Green: living cell. Red: dead cell; scale bar, 200 μm. (I) Quantification of living cells, statistic by Image J; *$P < 0.05$ and ****$P < 0.0001$(n = 3). (J) Quantification of loading cells in different culture models, statistic by Image J; ****$P < 0.0001$ (n = 3). (K) Quantification of proliferation cells in different culture models, statistic by Image J; ** $P < 0.01$ and **** $P < 0.0001$ (n = 3). (L) The gene of αSMA, Ki67, CK18 and AQP5 expression. * $P < 0.05$, ** $P < 0.01$, *** $P < 0.001$, and **** $P < 0.0001$, n.s. means not significant (n = 3). (M) Cytoskeleton staining. Green (Phalloidin): cytoskeleton; blue (DAPI): nucleus; scale bar, 200 μm. White dotted box is the enlarged area, scale bar, 100 μm. (N) The cumulative release of EGF of epithelial cells for 1, 3, 5, and 7 days. All results were analyzed with one-way ANOVA and Tukey's post-hoc multiple comparisons tests in GraphPad Prism 8. Results of 3D Encapsulation *vs.* 2D Surface, 3D Printing *vs.* 2D Surface and 3D Printing *vs.* 3D Encapsulation are shown in Figures I, J, K, and L.

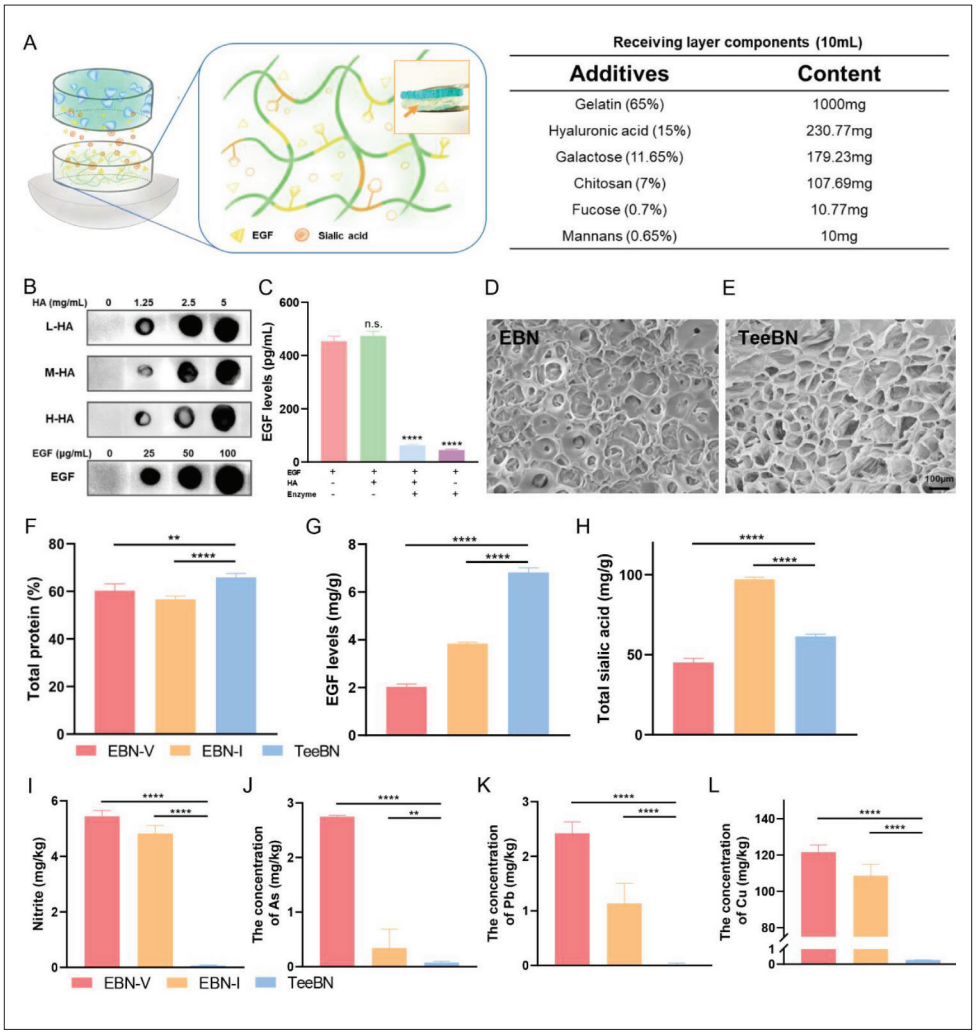

Figure 3. Preparation and evaluation of the receiving layer of TeeBN. (A) Schematic of receiving layer. Inset images showed the positional relationship: The blue upper layer is the feeding layer, and the white lower layer indicated by the orange arrow is the receiving layer. The table showed the main components of the receiving layer. (B) Dot blotting analysis of the binding between HA with different molecular weight and EGF with different concentration. (C) The EFG level after enzyme digested. ****$P < 0.0001$, n.s. means not significant (n = 5). (D) SEM image of EBN and (E) TeeBN. Scale bar, 100 μm. (F) The total protein content. **$P < 0.01$ and ****$P < 0.0001$ (n = 5). (G) The total EGF content. **** $P < 0.0001$ (n = 5). (H) The total sialic acid content. **** $P < 0.0001$ (n = 5). (I) The total nitrite content. **** $P < 0.0001$ (n = 5). (J) The heavy metal As (J), Pb (K), and Cu (L) content. **$P < 0.01$ and ****$P < 0.0001$ (n = 3). All results were analyzed with one-way ANOVA and Tukey's post-hoc multiple comparisons tests in GraphPad Prism 8 and expressed as mean ± SD. Results of TeeBN vs. EBN-V and TeeBN vs. EBN-I are show in Figures F to L.

charged carboxyl groups and is known for binding and storing growth factors in the extracellular matrix of mammalian tissue[31-33]. Meanwhile, HA forms hydrogel networks that helped to absorb the active substances released from the feeding layer and also provide mechanical supports[34]. In addition, as demonstrated by receiving layer components table in Figure 3A, we supplemented food-grade polysaccharides to complement the monosaccharide types mimicking the major carbohydrate ingredients found in natural EBN.

First, we screened HA of different molecular grades and concentrations for their capability to bind EGF. The dot-blotting assay showed that all HA of different sizes bound to EGF, and an increased dose of HA sequestered more EGF (Figure 3B). Meanwhile, the sequestered EGF could still be digested by the pepsin enzyme (Figure 2C), which is important because it indicated that the receiving layer could release this nutritious protein *in vivo* after being consumed. We selected 5% (w/v) HA (100–150 kDa) to prepare the receiving layer in this study.

During the TeeBN manufacturing process, the 0.4-μm pore polyester membrane trans-well system was used to distinguish layers. Specifically, the feeding layer was cultivated in round well, and the receiving layer in bottom

well. The grid feeding layer could greatly improve the survival rate of loading cells, and improve the nutrition exchange of cells in the center, which is more conducive to the release of active ingredients. More importantly, the 0.4-μm pore membrane could effectively inhibit cells' absconding from feeding layer into receiving layer.

Next, we characterized the receiving layer, which would become the final and edible product of TeeBN, in comparison to natural EBN. Scanning electron microscopy (SEM) revealed both had a porous network structure (Figure 3D and E), which is a key indicator in EBN authentication. Living cells were not present in the receiving layer, and no nucleic acid was found in the receiving layer (**Figure S1E**), both confirming there was no cell leaking from the feeding layer, thus eliminating the concern of exogenous animal cells in the edible product.

We determined the main nutritional substances and potentially toxic substances in TeeBN against two major, high-quality natural EBN products from Indonesia (EBN-I) and Vietnam (EBN-V), respectively. TeeBN contained more total proteins (65.32 ± 1.47%) than EBN-V (60.32 ± 2.57%, $P < 0.01$) and EBN-I (56.68 ± 1.21%, $P < 0.0001$; Figure 3F). Also, TeeBN had a significantly higher content of EGF (6.82 ± 0.17 mg/g) than EBN-V and EBN-I (2.03 ± 0.11 mg/g and 3.84 ± 0.05 mg/g, $P < 0.0001$, respectively; Figure 3G), which is both a main nutritional factor and a key marker in industrial EBN quality control. Further, the level of sialic acid in TeeBN (61.43 ± 1.23 mg/g) was higher than in EBN-V (45.28 ± 2.20 mg/g, $P < 0.0001$) and lower than in EBN-I (97.21 ± 1.15 mg/g, $P < 0.0001$; Figure 3H). For TeeBN, the concentration of the active ingredients could be further adjusted by changing the cell number in the feeding layer, providing extra controllability and convenience for product design.

Natural EBNs are inevitably contaminated with fungi, spores, nitrites, and heavy metals, and these substances are often detected in marketed products, including nitrite content 100-fold exceeding the safety standard in the so-called "rarest" blood EBN[8]. Fabricating TeeBN can avoid these risks completely. Nitrate was non-detectable in TeeBN, in sharp contrast to 5.45 ± 0.21 mg and 4.82 ± 0.29 mg per kg in EBN-V and EBN-I, respectively (Figure 3I). Almost no or only trace amounts of As, Pb, and Cu (all <0.5 mg/kg) were found in TeeBN, but were also present in considerable levels in both EBN-V and EBN-I. Notably, among them, the content of As and Pb in EBN-V reached 2.75 ± 0.03 mg/kg and 2.43 ± 0.21 mg/kg, respectively, which were 174.8% and 21.2% higher than the Bird's nest product verification implementation rules (CAIQ-RZ-2015002-7) issued by the China Academy of inspection and quarantine (Figure 3J–L)[35].

3.4. Metabolic profile analysis of EF-EBN and EBN

To comprehensively examine whether the cell-produced metabolites in TeeBN could, in full or part, resemble the bioactive ingredients of natural EBN, we performed an ultra-performance liquid chromatography-quadrupole time-of-flight mass spectrometry (UPLC-QTOFMS)-based metabolomics analysis. The outcomes identified 601 metabolites in the engineered TeeBN and the high-quality natural EBN-I (Venn diagram, Figure 4A). Among them, 265 metabolites were shared between two groups, demonstrating most EBN ingredients (85.76%) being produced in TeeBN. A PCA further revealed the differences (Figure 4B). The distribution areas of TeeBN and EBN were separated, indicating significant differences in the compositions. The PLS-DA model further highlighted the difference (**Figure S2A**), followed by a permutation test preventing the model from overfitting (**Figure S2B**). Based on the available model, the PLS-DA S-plot identified the characteristic metabolites between TeeBN and the natural EBN-I, located in the lower-left and upper-right corner and in total 222 (Figure 4C).

Further analysis into the top 19 discriminating metabolites between TeeBN and EBN-I demonstrated that 18 were higher in the former (Figure 4D and **Figure S2C**). Notably, two discriminating metabolites, *N*-Acetyl-9-O-acetylneuraminic acid and *N*-Acetyl-7-O-acetylneuraminic acid, belong to sialic acids, which echoed with the above data on determining sialic acids, which is a key quantitative index for assessing EBN quality (Figure 4E–I). Finally, a full picture of the metabolic pathways of TeeBN and natural EBN-I was analyzed. As shown in Figure 4J, TeeBN mainly influenced the pathways of metabolism, organismal system, and environmental information processing pathway ($P < 0.05$ and pathway impact >0), with significant influences on amino acid metabolism, the digestive system, biosynthesis of other secondary metabolites, and membrane transport. In summary, TeeBN shared many nutritional factors including vitamins, amino acids, monosaccharides, cofactors, fatty acids, phospholipids, nucleosides, and carboxylic acids[36]. Its similarity with natural EBN-I in metabolite patterns suggested that TE-based production by epithelial cells resembled the natural process.

3.5. Blood serum metabolomics

Finally, we tested in mice how TeeBN as a potential food was metabolized *in vivo* by examining the blood serum metabolomics in mice (Figure 5A). In total, 10,625 peaks were detected in the control, TeeBN and natural EBN groups. Among them, 185 metabolites were identified in comparison to established databases (Figure 5B). PCA revealed high similarity among the profiles of serum metabolites of these

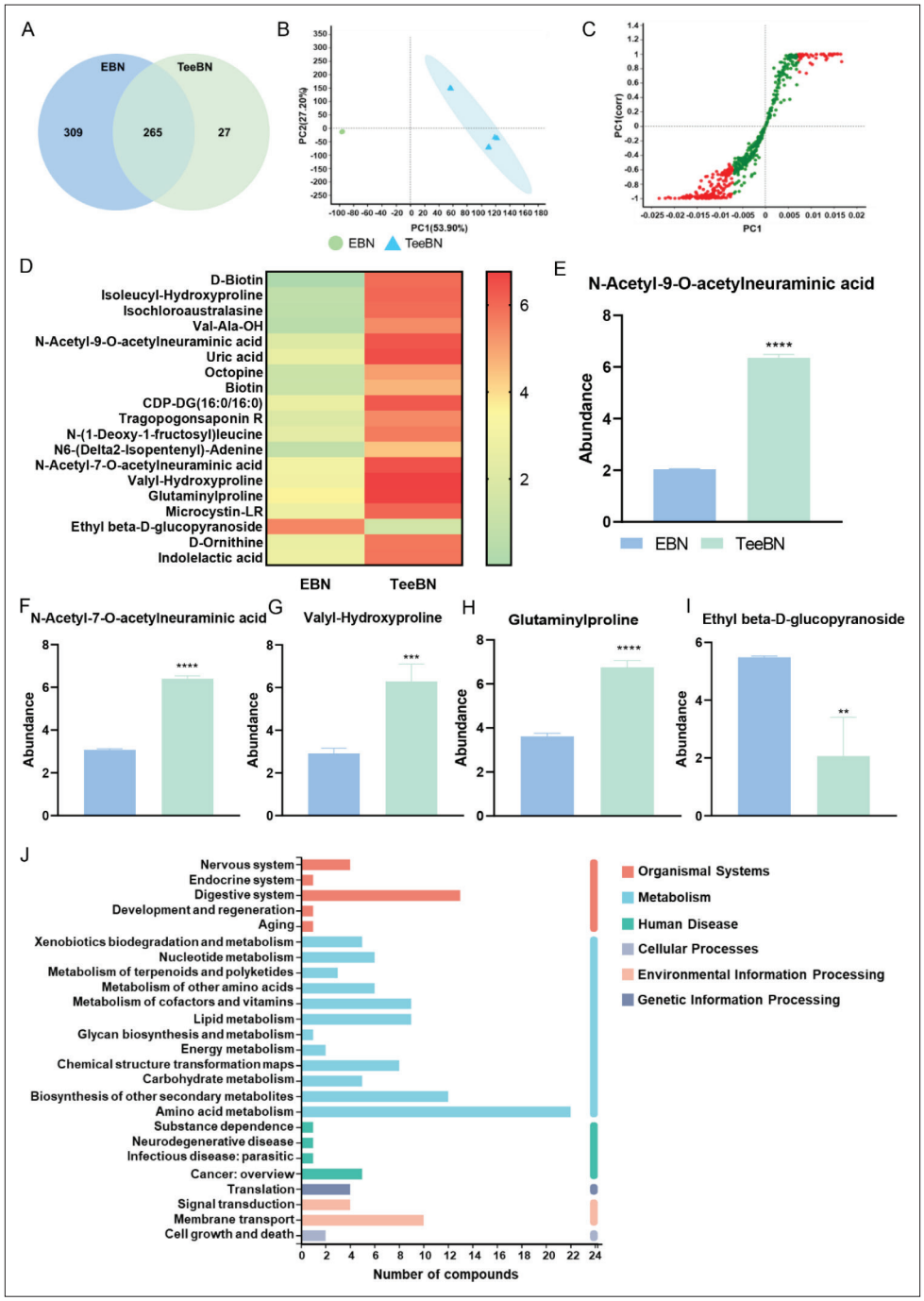

Figure 4. Metabolic profile analysis of one natural EBN product from Indonesia and TeeBN. (A) Venn diagram of metabolites in EBN and TeeBN group. (B) Principal component analysis. (C) S-plot derived from the orthogonal partial least squares-discriminate analysis. (D) Heat map for comparison of the abundance of top 19 discriminating metabolites in TeeBN and EBN. Quantification representative discriminating metabolites of *N*-Acetyl-9-O-acetylneuraminic acid (E), *N*-Acetyl-7-O-acetylneuraminic acid (F), Valyl-Hydroxyproline (G), Glutaminylproline (H), and ethyl beta-D-glucopyranoside (I). $^{**}P < 0.01$, $^{***}P < 0.001$, and $^{****}P < 0.0001$ (n = 6). (J) KEGG metabolic pathway enrichment revealed the biological activities of major metabolites. All results were analyzed with paired *t*-tests in GraphPad Prism 8. Results of TeeBN vs. EBN are shown in Figures E to I.

three groups, and the two sample groups (TeeBN and natural EBN from Indonesia) were closer and more similar in terms of the profile of serum metabolites; however, EBN and TeeBN were all significantly different from the control group. This result showed that in the process of *in vivo* metabolism, TeeBN can simulate EBN to a certain extent (Figure 5C). Despite minor overlaps in PLS-DA, a distinct separation of the serum metabolites existed among

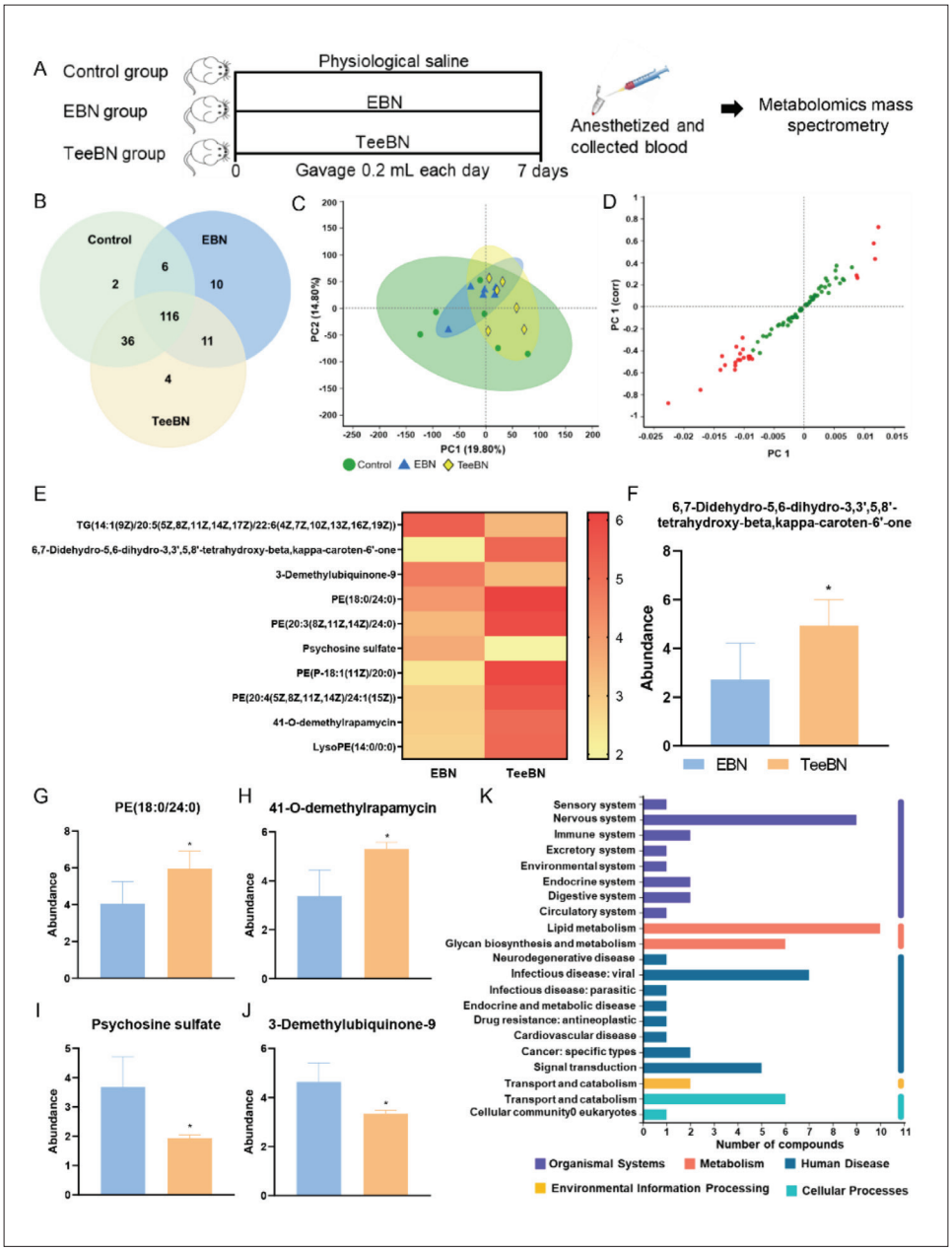

Figure 5. Serum metabolic profile analysis of one natural product of EBN from Indonesia and TeeBN. (A) Schematic illustration of the *in vivo* study: 0.2 mL physiological saline (n = 6) or EBN (n = 6) or TeeBN (n = 6) were treated by gavage, once a day. After 7 days, blood was collected for plasma metabolomics testing. (B) Venn diagram of metabolites in control, EBN, and TeeBN group. (C) Principal component analysis. (D) S-plot derived from the orthogonal partial least squares-discriminate analysis. (E) Heat map for comparison of the abundance of top 10 discriminating metabolites in TeeBN and EBN. Quantification representative discriminating metabolites of (F) 6,7-Didehydro-5,6-dihydro-3,3',5,8'-tetrahydroxy-beta, kappa-caroten-6'-one, (G) PE (18:0/24:0), (H) 41-O-demethylrapamycin, (I) Psychosine sulfate, and (J) 3-Demethylubiquinone-9. *$P < 0.05$ (n = 6). (K) KEGG metabolic pathway enrichment revealed the biological activities of major metabolites. All results were analyzed with paired *t*-tests in GraphPad Prism 8. Results of TeeBN *vs.* EBN are shown in Figures F to J.

the three groups (**Figure S3A**), showing a great extent of similarity between the metabolic profiles of the natural EBN and their engineered counterparts. Nevertheless, we performed orthogonal projections to latent structures discriminant analysis (OPLS-DA) to further examine their differences (**Figure S3B**), with S-plot identifying the discriminating metabolites (Figure 5D). From the top 10 discriminating serum metabolites between TeeBN and EBN-I groups (Figure 5E–J and **Figure S3C**), we noted that the most discriminating serum metabolites belonged

to phospholipids, demonstrating that the engineered and natural EBN regulated lipid metabolism to varying degrees. These outcomes might add weight to previous findings that EBN intake could inhibit high fat diet-induced oxidative stress and insulin resistance, potentially attenuating the coagulation effects of high-fat diets *in vivo*[37,38].

The KEGG enrichment analysis revealed the metabolic mechanism differences between the two groups. As shown in Figure 5K, the serum metabolic pathways ($P < 0.05$ and pathway impact >0) influenced by our new approach mainly focused on metabolism, organismal system, and human diseases pathways, with lipid metabolism, glycan biosynthesis and metabolism, nervous system, and infectious disease (viral) significantly upregulated.

Overall, the data indicated that the intake of TeeBN had highly similar effects compared with the natural EBN-I, from a metabolomics perspective. The only detectable differences were limited to a few aspects, such as lipid metabolism[37,39]. These findings again proved our assumption that TeeBN had the potential to provide a comparable nutritional value as natural EBN, while preventing the huge environmental costs rendered by wild harvesting.

Our study resonates with recent works in the field of cellular agriculture, represented by cell-based meat, which "grows" animal-based products from mammalian cell culture instead of harvesting from live animals[40]. In 2020, Singapore approved the world's first cell-cultured chicken for sale, which is seen as a landmark moment for the future lab-grown meat industry[41]. Based on the production process of TeeBN, TeeBN products are expected to have more market opportunities. For example, different from cell-cultured meat production, living cells in fabricating TeeBN only serve to secrete the active ingredients from the feeding layer. The cells are excluded from the receiving layer and do not become part of the final products. In this regard, TeeBN would encounter fewer regulatory hurdles for premarket approvals than cell-cultured meat in many jurisdictions, even in the European Union, where the authority has adopted possibly the most stringent regulations on novel foods globally[42]. Moreover, the manufacturing process of TeeBN will dramatically reduce the risk of human–animal disease transmission and exposure to harmful heavy metals, which will decrease public health and heavy metal poisoning risks. In addition, the open platform of the receiving layer allows for the easy addition of nutritional ingredients or even extra flavor condiments, enabling more tailored services that satisfy consumers' different demands.

Toward a successful commercialization of TeeBN, future research can focus on several possibilities. The first is on better control of the release kinetics of the active components from the feeding layer and the loading capacity of the receiving layer, with attention to possible loss during this process. Second, we used laboratory cell culture in this proof-of-concept study, while in future scale-up scenarios, bioreactors and related facilities are required for maintaining high viability of large cell numbers. Third, culturing of either primary or immortalized cells of multiple species could be compared, taking into account the production (e.g., cost, manufacturing) issues. Last but not the least, discussions on legal and ethical issues associated with the TeeBN should be further developed such as what food safety monitoring systems should be established to ensure the quality of TeeBN products, and how to label TeeBN products that can accurately describe features of the product and protect consumers from misleading advertisement.

4. Conclusion

Our study demonstrated a prototype of substitutes for natural EBN based on *in vitro* culture of epithelial cells in 3D-printed matrices, inspired by the tissue engineering technology that grows human tissue cells in biomaterials scaffolds. We focused on evaluation of the viability and secretion functionality of epithelial cells in the engineered matrices, termed as the feeding layer, which ensured the production of nutritional factors mimicking the natural process carried out in the salivary gland of the birds. We also highlighted that such factors could smoothly diffuse from the feeding layer to a receiving layer with well-defined, food-scale components. The final products preserved the main ingredients traditionally assumed to be nutritional in natural EBN, including EGF and sialic acids, while avoiding contamination of harmful microbial and chemical substances. The engineered products had a similar metabolic profile as natural EBN in mice, thereby showing the potential to reduce or replace excessive farming of wild bird's nests that is accompanied by huge environmental and ecological costs. Further, biotechnological, ethical, and legal investigations are required to accelerate development of such products toward commercialization.

Acknowledgments

We thank Ms. Ruoyu Mu and Mr. Zhencheng Liao for technical discussion on *in vivo* experiments and 3D printing, respectively.

Funding

This study was funded by the Science and Technology Development Fund, Macau SAR (File no. 0060/2020/AGJ and 0097/2019/A2), Shenzhen-Hong Kong-Macau Science and Technology Program Category C (SGDX20201103092803014) of the Shenzhen Science

and Technology Innovation Commission, and "Excellent Young Scientist Fund" of the National Natural Science Foundation of China (32022088).

Conflict of interest

The authors declare no conflicts of interest.

Author contributions

Conceptualization: Chunming Wang.
Formal analysis: Yu Liu, Yangyang Liu
Investigation: Yu Liu, Yangyang Liu, Jiayue Liu, Jianbo Wan, Yuwei Li, Yiming Niu
Writing – original draft: Yu Liu, Lei Dong, Li Du, Chunming Wang
Writing – review & editing: Chunming Wang and Li Du.

Ethics approval and consent to participate

This study was reviewed and approved by the Ethics Committee of the University of Macau (UMARE-03-2017 and UMARE-006-2022). All protocols met the requirements of the National Institutes of Health (NIH) Guide for the Care and Use of Laboratory Animals.

Consent for publication

Not applicable.

Availability of data

Data are available from the corresponding author upon reasonable request.

References

1. Lee TH, Wani WA, Lee CH, *et al*., 2021, Edible bird's nest: The functional values of the prized animal-based bioproduct from southeast Asia—A review. *Front Pharmacol*, 12:626233.
2. Marcone MF, 2005, Characterization of the edible bird's nest the "Caviar of the East." *Food Res Int*, 38(10):1125–1134.
3. Edible Bird's Nest Market Committee of China Agricultural Wholesale Markets Association, 2019, White paper of edible bird's nest industry 2019. viewed July 07, 2022, http://www.cawa-ebmc.org/index.php?c=content&a=show&id=1161
4. China Academy of Inspection and Quarantine, 2021, 2020 Bird's Nest Traceability Report, viewed July 07, 2022, https://www.caiq.org.cn/haccp/jsfw/2021/07/905729.shtml
5. Wikipedia. Edible bird's nest. Available from: https://en.wikipedia.org/wiki/Edible_bird%27s_nest.
6. PER LILJAS, B., How the ancient practice of harvesting edible bird's nests is facing some very modern challenges, in *TIME*. December 25, 2015.
7. Johnson NC, Haig SM, Mosher SM, *et al*., 2017, Reproductive success of Mariana Swiftlets (*Aerodramus bartschi*) on the Hawaiian island of O'ahu. *J Field Ornithol*, 88(4): 362–373.
8. Yeo BH, Tang TK, Wong SF, *et al*., 2021, Potential residual contaminants in edible bird's nest. *Front Pharmacol*, 12:631136.
9. Shim EK-S, Lee S-Y, 2018, Nitration of tyrosine in the mucin glycoprotein of edible bird's nest changes its color from white to red. *J Agric Food Chem*, 66(22):5654–5662.
10. Berthiaume F, Maguire TJ, Yarmush ML, 2011, Tissue engineering and regenerative medicine: History, progress, and challenges. *Ann Rev Chem Biomol Eng*, 2(1):403–430.
11. Ma F, Liu D, 2012, Sketch of the edible bird's nest and its important bioactivities. *Food Res Int*, 48(2):559–567.
12. Daud NA, Yusop SM, Babji AS, *et al*., 2021, Edible bird's nest: physicochemical properties, production, and application of bioactive extracts and glycopeptides. *Food Rev Int*, 37(2):177–196.
13. Yue K, Santiago GT, Alvarez MM, *et al*., 2015, Synthesis, properties, and biomedical applications of gelatin methacryloyl (GelMA) hydrogels. *Biomaterials*, 73:254–271.
14. Fang X, Zhong X, Xie L, *et al*., 2016, Biomimetic gelatin methacrylamide hydrogel scaffolds for bone tissue engineering. *J Mater Chem B*, 4(6):1070–1080.
15. Liao Z, Niu Y, Wang Z, *et al*., 2022, A "nonsolvent quenching" strategy for 3D printing of polysaccharide scaffolds with immunoregulatory accuracy. *Adv Sci*, 9(34):e2203236.
16. Mu R, Zhang Y, Yan L, *et al*., 2021, A "bridge-building" glycan scaffold mimicking microbial invasion for in situ endothelialization. *Adv Mater*, 33(42):2103490.
17. Li X, Wu M, An D, *et al*., 2019, Suppression of Tafazzin promotes thyroid cancer apoptosis via activating the JNK signaling pathway and enhancing INF2-mediated mitochondrial fission. *J Cell Physiol*, 234(9):16238–16251.
18. Niu Y, Wang L, Yu N, *et al*., 2020, An "all-in-one" scaffold targeting macrophages to direct endogenous bone repair in situ. *Acta Biomater*, 111:153–169.
19. Kathan RH, Weeks DI, 1969, Structure studies of collocalia mucoid: I. Carbohydrate and amino acid composition. *Arch Biochem Biophys*, 134(2):572–576.
20. Tokalıoğlu Ş, 2012, Determination of trace elements in commonly consumed medicinal herbs by ICP-MS and multivariate analysis. *Food Chem*, 134(4):2504–2508.
21. Tian X, Yan Y, Yan F, 2020, The method of measuring nitrite by iodometry. *Adv in Anal Chem*, 10(3):74–79.
22. Stelfox AJ, Bowden TA, 2019, A structure-based rationale for sialic acid independent host-cell entry of Sosuga virus. *Proc Natl Acad Sci*, 116(43):21514–21520.

23. Zhang A, Sun H, Wang X, 2012, Serum metabolomics as a novel diagnostic approach for disease: A systematic review. *Anal Bioanal Chem*, 404(4):1239–1245.

24. Zelena E, Dunn WB, Broadhurst D, *et al*., 2009, Development of a robust and repeatable UPLC– MS method for the long-term metabolomic study of human serum. *Anal Chem*, 81(4):1357–1364.

25. Tabatabaei F, Moharamzadeh K, Tayebi L, 2020, Fibroblast encapsulation in gelatin methacryloyl (GelMA) versus collagen hydrogel as substrates for oral mucosa tissue engineering. *J Oral Biol Craniofac Res*, 10(4):573–577.

26. PT, JB, 2020, Bioprinting Protocol: CELLINK GelMA, viewed July 07, 2022, https://www.cellink.com/wp-content/uploads/2022/03/Bioprinting-protocol-GelMA_18-Dec-2020-5.pdf

27. Ouyang L, *et al*., 2016, Effect of bioink properties on printability and cell viability for 3D bioplotting of embryonic stem cells. *Biofabrication*, 8(3):035020.

28. Thiemann RF, Varney S, Moskwa N, *et al*., 2021, Regulation of myoepithelial differentiation in 3-dimensional culture. *bioRxiv*. https://doi.org/10.1101/2021.06.28.450182.

29. Shin HS, Hong HJ, Koh WG, *et al*., 2018, Organotypic 3D culture in nanoscaffold microwells supports salivary gland stem-cell-based organization. *ACS Biomater Sci Eng*, 4(12):4311–4320.

30. Petrakova OS, Terskikh VV, Echernioglo ES, *et al*., 2014, Comparative analysis reveals similarities between cultured submandibular salivary gland cells and liver progenitor cells. *Springerplus*, 3:183.

31. Hintze V, Schnabelrauch M, Rother S, 2022, Chemical modification of hyaluronan and their biomedical applications. *Front Chem*, 10:830671.

32. Macri L, Silverstein D, Clark RAF, 2007, Growth factor binding to the pericellular matrix and its importance in tissue engineering. *Adv Drug Deliv Rev,* 59(13):1366–1381.

33. Zhang F, Zheng L, Cheng S, *et al*., 2019, Comparison of the interactions of different growth factors and glycosaminoglycans. Molecules (*Basel, Switzerland*), 24(18):3360.

34. Xu X, Jha AK, Harrington DA, *et al*., 2012, Hyaluronic acid-based hydrogels: From a natural polysaccharide to complex networks. *Soft Matter*, 8(12):3280–3294.

35. China Academy of Inspection and Quarantine, 2020, Bird's nest product certification implementation rules, CAIQ-RZ-2015002-7, amended March 16, 2020, *Chinese Bird's Nest Traceability Management Service Platform*, viewed July 07, 2022.

36. Chye SM, Tai SK, Koh RY, *et al*., 2017, A mini review on medicinal effects of edible bird's nest. *Lett Health Biol Sci*, 2(1):65–67.

37. Yida Zhang, Imam MU, Ismail M, *et al*., 2015, Edible bird's nest attenuates high fat diet-induced oxidative stress and inflammation via regulation of hepatic antioxidant and inflammatory genes. *BMC Complement Altern Med*, 15(1):310.

38. Yida zhang, Iman MU, Ismail M, *et al*., 2015, Edible bird's nest prevents high fat diet-induced insulin resistance in rats. *J Diabetes Res*, 2015:760535.

39. Chok KC, Ng MG, Ng KY, *et al*., 2021, Edible bird's nest: recent updates and industry insights based on laboratory findings. *Front Pharmacol*, 12:746656.

40. Ben-Arye T, Shandalov Y, Ben-Shaul S, *et al*., 2020, Textured soy protein scaffolds enable the generation of three-dimensional bovine skeletal muscle tissue for cell-based meat. *Nat Food*, 1(4):210–220.

41. Guardian T, 2020, No-kill, lab-grown meat to go on sale for first time. Available from: https://www.theguardian.com/environment/2020/dec/02/no-kill-lab-grown-meat-to-go-on-sale-for-first-time

42. Organisms E.P.o.G.M., 2011, Guidance on the risk assessment of genetically modified microorganisms and their products intended for food and feed use. *EFSA J*, 9(6):2193.